Temperature-dependent 780-nm laser absorption by engineering grade aluminum, titanium, and steel alloy surfaces

Alexander M. Rubenchik
Sheldon S. Q. Wu
V. Keith Kanz
Mary M. LeBlanc
W. Howard Lowdermilk
Mark D. Rotter
Joel R. Stanley

Temperature-dependent 780-nm laser absorption by engineering grade aluminum, titanium, and steel alloy surfaces

Alexander M. Rubenchik, Sheldon S. Q. Wu,* V. Keith Kanz, Mary M. LeBlanc, W. Howard Lowdermilk, Mark D. Rotter, and Joel R. Stanley
Lawrence Livermore National Laboratory, Livermore, California 94550, United States

Abstract. The modeling of laser interaction with metals for various applications requires a knowledge of absorption coefficients for real, commercially available materials with engineering grade (unpolished, oxidized) surfaces. However, most currently available absorptivity data pertain to pure metals with polished surfaces or vacuum-deposited thin films in controlled atmospheres. A simple laboratory setup is developed for the direct calorimetric absorptivity measurements using a diode-array laser emitting at 780 nm. A scheme eliminating the effect of convective and radiative losses is implemented. The obtained absorptivity results differ considerably from existing data for polished pure metals and are essential for the development of predictive laser-material interaction models. © *2014 Society of Photo-Optical Instrumentation Engineers (SPIE)* [DOI: 10.1117/1.OE.53.12.122506]

Keywords: thermal effects; laser arrays; metals.

Paper 140398 received Mar. 10, 2014; revised manuscript received Jun. 2, 2014; accepted for publication Jun. 17, 2014; published online Jul. 17, 2014.

1 Introduction

Measurement of absorptivity is important for analysis and modeling of laser-material interactions. Absorption of laser light depends on the laser parameters: irradiance, wavelength, polarization, and angle of incidence; and material properties including composition, temperature, surface roughness, oxide layers, and contamination. Theoretical and experimental studies of absorptivity and reflectance of metals have concentrated on perfectly pure, clean, and flat surfaces, free of oxide layers, unlike real life material processing applications where metal surfaces are rough to some extent and are contaminated with impurities and oxide layers. Furthermore, little information is available on absorptivity of alloys, which are far more commonly used than pure metals in real processing applications. Thus the published values of absorptivity for pure polished surfaces are inadequate for laser-material interaction models. In addition, detailed analysis and modeling of laser-material interactions require material absorptivity over a wide range of temperatures. The standard collection of textbooks[1] has data mainly for ideal materials at room temperature. In engineering applications, metals are oxidized and have impurities, surface irregularities, and defects; hence, their absorptivity can be considerably different from handbooks' values.[2]

Lasers have been widely used for many years in various material processing applications. In situations that do not require narrow linewidth laser beams where the laser acts as an energy source only, the more energy-efficient diode-array lasers can be used. Such lasers are now commercially available in a wide variety of wavelengths and formats and were used as radiation sources in these experiments.

Direct absorptivity measurements are difficult due to the need to change the sample temperature in controlled way.

Absorptivity is usually determined indirectly as the residual of the measured reflectivity.[3] However, reflectance is difficult to measure accurately due to diffuse scattering and thermal radiation, especially for measurements at high temperatures. To avoid these problems, direct calorimetry was used here in which a thin sample is heated uniformly by a diode array and the temperature evolution is measured using thermocouples and (or) an infrared camera. The small thickness provides a temperature uniformity across the sample. Heat losses due to convection and thermal radiation are derived directly from the experimental data and, by removing this contribution, the temperature-dependent absorptivity at a wavelength of 780 nm is obtained. In addition, the measurements of thermal loss as a function of temperature, containing information about both convective loss and thermal radiative loss, are also discussed. The simple and compact setup, together with new way of data processing, is a convenient tool for temperature-dependent absorptivity measurements for engineering applications.

This study focuses on the absorptivity of aluminum, while some data for titanium and steel are also presented. Extensive previous theoretical and experimental works on aluminum allow comparison of absorptivity for the engineering grade samples and ideal metals. The various mechanisms that increase absorptivity in real materials are discussed. Measurement results for steel and Ti alloys are also presented. It is demonstrated that the oxidation process is nonuniform and lead to variations in absorptivity across the illuminated area.

2 Experimental Setup and Measurement Procedure

For direct, calorimetric absorptivity measurements, a thin sample is heated by the diode laser array and temperature evolution is measured using thermocouples, as illustrated schematically in Fig. 1. The sample is thermally isolated
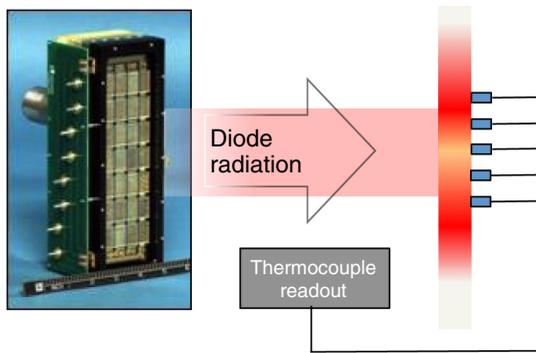

Fig. 1 Experimental arrangement. Light from a diode laser array is transported optically (not shown) to a metal sample with attached thermocouples.

and all heating is produced by the absorption of laser light. The irradiation is approximately uniform over the sample. The small sample holder was made from fused silica, which has minimal absorption of laser light. Thermal measurements indicate a high degree of uniformity over the sample. At some moment, the radiation is turned off and the sample cools via thermal radiation and convection cooling. For the thin samples used, the thermal diffusion time is much shorter than the heating time, so the temperature is expected to be uniform throughout the sample. The temperature-dependent absorptivity $A(T)$ for a sample with uniform temperature distribution (uniform irradiation and thin sample) is determined by the relation

$$w\rho(T)c_{\mathrm{P}}(T)\frac{\partial T}{\partial t} = A(T)I - Q(T), \qquad (1)$$

where w is the sample thickness, $\rho(T)$ is the density, $c_{\mathrm{p}}(T)$ is the temperature-dependent specific heat, I is the incident intensity, and $Q(T)$ is the thermal loss. Assuming thermal loss is a function only of sample temperature, i.e., the loss channels are identical with and without laser illumination, and the $Q(T)$ measured during cooling when the laser is off also applies during heating, then the absorptivity of the sample can be determined with the minimal ambiguity.[2]

Square samples of industrial grade aluminum, 1-mm thick and 3×3-cm wide, were used in these measurements. The diode-array laser produced up to 3-kW power at 780 nm. Radiation was transported to the target through a fused silica "duct" that spatially smoothed the irradiance distribution, as shown in Fig. 2, by multiple reflections from the walls to a
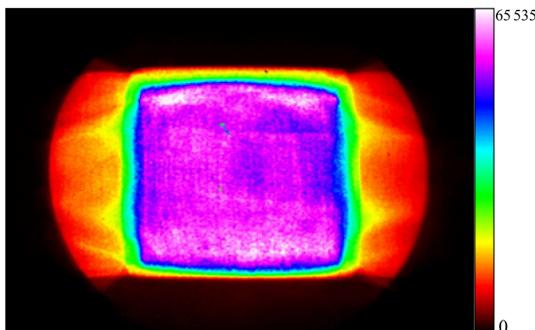
uniformity of $\pm5\%$. Irradiance on the sample was limited to 10 to 40 W/cm^2 to heat the target slowly enough for convective cooling to be in a steady-state regime and to improve the temporal resolution of temperature recording. The sample temperature was measured by up to five thermocouples distributed over the surface to verify the uniformity of the temperature, as shown in Fig. 3 where typical data from five different thermocouples are presented. The thermocouples used were type K with an expected measurement accuracy within 3°C and a response time well under a second.

The parameters $Q(T)$ and $A(T)$ are calculated from the time derivative of the measured sample temperature, which is difficult to do accurately when the data are noisy. To improve the numerical accuracy, data smoothing techniques described in Appendix A were applied.

Measurements were made over a sufficiently broad range of sample temperatures; hence, it was necessary to account for the temperature dependence of the density and heat capacity of the metal sample. Data from Ref. 4, shown graphically in Fig. 4, were used. A polynomial curve fit for the density gives $\rho(T) = M_0 + M_1 T$ with $M_0 = 2.71$, $M_1 = -0.0002$, and a correlation coefficient $R = 0.997$. Similarly, the fitted curve for specific heat capacity gives $c_{\mathrm{P}}(T) = M_0 + M_1 T + M_2 T^2 + M_3 T^3$ with $M_0 = 0.841$, $M_1 = 0.00139$, $M_2 = -4.39 \times 10^{-6}$, $M_3 = 5.70 \times 10^{-9}$, and $R = 0.998$.

The resulting thermal loss curves, $Q(T)$, calculated for several Al targets heated with laser irradiances of 12 and 24 W/cm^2 in various heating experiments, shown in Fig. 5, demonstrate high repeatability and show that the thermal loss is a function only of the temperature that is independent of the heating rate. Smoothing and processing of measured temperatures does not result in a significant deviation in the results. Small differences between each curve may be attributed to environmental fluctuations in the experimental area. One example is the position and orientation of the thermocouple wires. Because the thermocouple wires were not attached and positioned exactly in the same way in every experiment, their influence on thermal convection will vary from experiment to experiment. The increase in variation at higher temperatures is also consistent with this explanation. An approximate deviation on the order of 0.2 W/cm^2 for $Q(T)$ would result in an error of 5% or less for the absorptivity—comparable to the accuracy of measurement.

Fig. 2 Measured irradiance profile of diode laser source at the target plane.
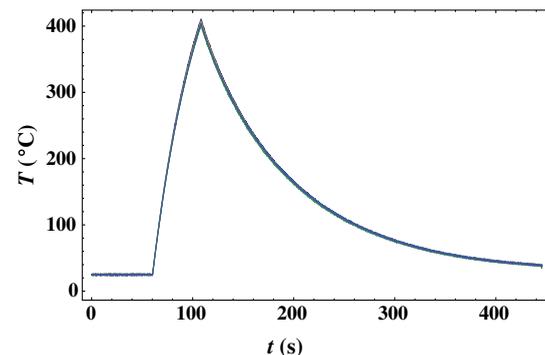

Fig. 3 Temperature data recorded from five different thermocouples on a typical fresh aluminum sample. The measured temperatures from the different thermocouples are nearly identical and any difference is not visible on this scale.
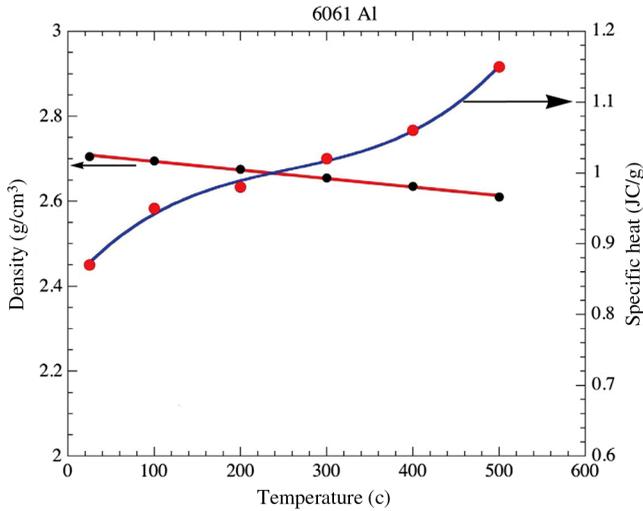
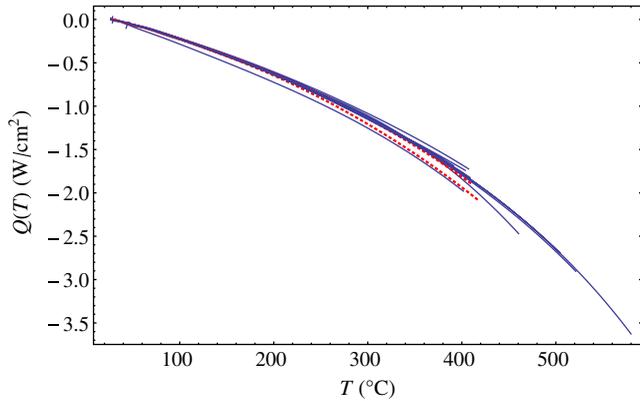**Fig. 4** Density (red) and specific heat (blue) for aluminum 6061.[4]

Fig. 5 $Q(T)$ calculated from a number of different experiments on aluminum 6061 at two different intensities: 12 and 24 W/cm^2 (dashed).

3 Absorptivity of Aluminum

A comparison of absorption of Al alloys before and after correction for thermal loss, shown in Fig. 6, illustrates the importance of accounting for thermal losses. The loss-corrected results are found to be only weakly dependent on heating rate, jus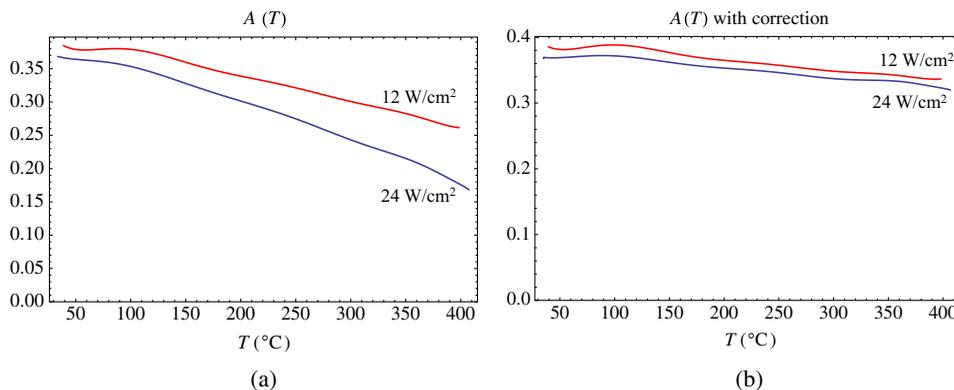tifying our approach. The absorptivity for Al is about 35% and is nearly constant over this temperature range. Heating to 450°C did not produce a significant change in sample appearance or morphology, and the repetitive measurements produced similar results. An estimated energy measurement error of 5% is expected due to thermopile heat sensor sensitivity and laser beam nonuniformity. The scheme for the removal of thermal losses may result in another 5% numerical error in absorptivity as stated above. Hence, one should expect a relative accuracy better than 10% for the derived absorptivity.

Absorption data for Al presented in textbooks[1] are measured for ideal, vacuum-deposited films. Measurements here on as received, engineering grade, plate aluminum samples show much higher absorption, which is usually attributed to surface roughness, the presence of oxide films, and absorbing impurities.[2] The comparative magnitude of these effects and their wavelength dependence is discussed below.

Aluminum is one of the so-called near-free-electron metals, for which electrons in the metal can be treated as a free-electron gas, with the addition of interband transitions.[2] The Drude model provides a good description of the dielectric constant. Figure 7 shows the pure Al absorption as a function of wavelength for irradiation at normal incidence based on the experimental measurements of the refractive index.

Absorption typically increases with temperature, except for the resonance region, simply because the free electrons gain kinetic energy while the phonon population grows, which increases the electron-phonon collision frequency. Aluminum has an absorption peak at 820 nm due to an interband transition, which is clearly shown by the blue line in Fig. 7. Absorption at 795 nm ($n = 2.767 + 8.48i$) is about 13%, and 2.5 times higher than the absorption at 1 μm ($n = 1.27 + 10.41i$), while for 1.3-μm light ($n = 1.23 + 13.46i$) absorption falls to 2.7%. Absorption data for liquid Al (red dots in Fig. 7) show that the elimination of the metal structure makes absorptivity insensitive to wavelength.

Experimental data presented for 1-μm radiation absorption of bulk Al[2] demonstrates very different results, with absorption more than four times higher than that measured for the ideal sample.[1] Also, the absorption is nearly temperature independent.

In real situations, aluminum is coated with an oxide layer that is transparent up to the UV range but has a high refractive index, $n = 1.62$ for a wavelength of 0.78 μm,[2] that can

Fig. 6 Absorption data before (a) and after (b) removal of thermal losses. The red curves correspond to absorptivity measured under 12 W/cm^2 irradiance and blue curves under 24 W/cm^2. Small differences can be attributed to the sample differences or measurement error.
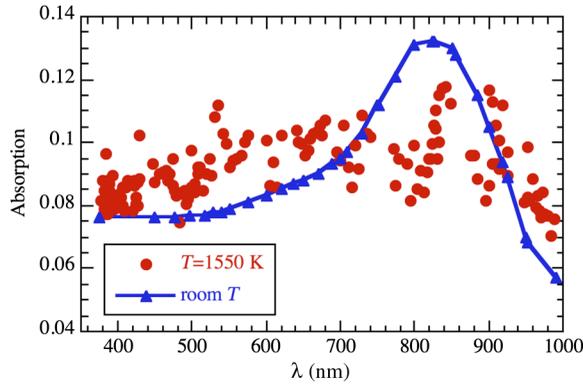
Fig. 7 Experimental data of absorption versus wavelength for light incident normally on aluminum at room temperature (blue curve presents the data taken from Ref. 1) and at 1550 K (red circles are taken from Refs. 5 and 6).

affect the reflectivity. The complex amplitude r of a wave reflected from the oxide film of thickness h on the aluminum substrate is given by[7]

$$r = \frac{r_{12}e^{-2i\varphi} + r_{23}}{e^{-2i\varphi} + r_{12}r_{23}}, \qquad \varphi = \frac{\omega h}{c}\sqrt{n^2 - \sin^2\theta}. \qquad (2)$$

Here, n is the oxide refractive index and $n_3 = 2.767 + 8.48i$ is the complex refractive index of Al; r_{12} is the amplitude of the wave reflected from the bulk aluminum oxide, given by $r_{12} = (1 - n)/(1 + n) = -0.24$, r_{13} is the complex reflected amplitude from the bulk aluminum material, and θ is the angle of incidence. The complex value r_{13} is $r_{13} = (1 - n_3)/(1 + n_3) = -0.91 - 0.20i$. Reflectivity from bulk Al at this wavelength is $R = |r_{13}|^2 = 0.87$ and absorptivity $A = 1 - R = 0.13$. The value for r_{23} is given by $r_{23} = (r_{12} - r_{13})/(r_{12}r_{13} - 1) = -0.84 - 0.30i$. For the p-polarized wave, all data are related to the magnetic field amplitude and the electric field amplitude for the s-polarized wave.

In the case of normal incidence, the calculated absorptivity as a function of the oxide layer thickness is shown in Fig. 8, which shows that the presence of an oxide layer can substantially increase absorption. For a typical thickness of about 50 nm, absorption will be above 20%. Variability of the thickness will result in some average absorption value, but it will be higher than that predicted for pure aluminum.
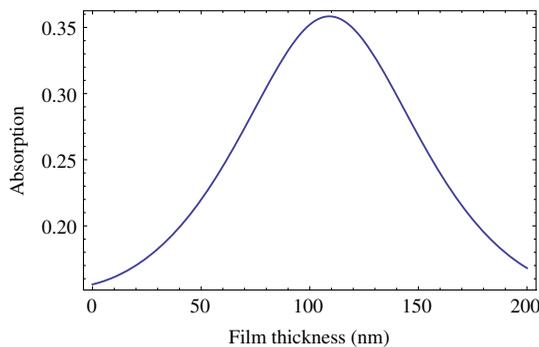

Fig. 8 Calculated absorptivity curve of Al coated by oxide film as a function of film thickness.
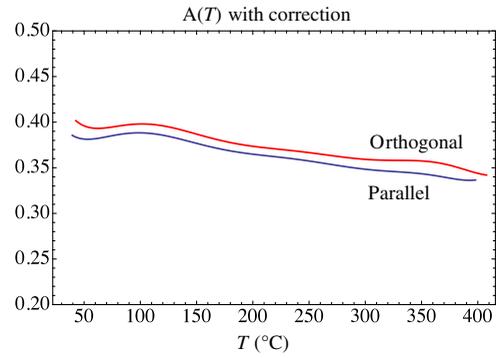

Fig. 9 Absorptivity measurements with light polarized parallel (blue) and orthogonal (red) to the grooves direction. The irradiance in both cases was 12 W/cm².

The reduction in absorptivity for a thicker oxide film, shown in Fig. 8, is the result of wave interference in the film.

Thus, the presence of an oxide film increases the absorptivity but not sufficiently to explain the observed results. The effect of the oxide layer is more noticeable for shorter wavelength light. The additional absorption is explained by the surface roughness resulting in enhanced absorption and conversion of incident radiation to surface electromagnetic waves (plasmons). General calculations of absorption on a rough metal surface can be found, e.g., in Ref. 2, but are not helpful because detailed information about the surface structure is not usually available. Other possibilities are the surface defects and inclusions.[2]

The cold-rolled samples used for these measurements have parallel groves in the roll direction. Figure 9 shows the absorption measured with the electric field of the light parallel or orthogonal to the grooves. The higher absorption observed for the orthogonal field orientation is due to the fact that it is p-polarized with respect to the corrugated surface, thus having higher absorption than the parallel field which is s-polarized. These data directly demonstrate the effect of surface corrugations.

Heating the samples to 400°C does not cause irreversible material changes in Al, as repetitive measurements on the same sample gave similar results and no visible changes were observed on the surface. However, when samples were heated close to their melting temperature, or
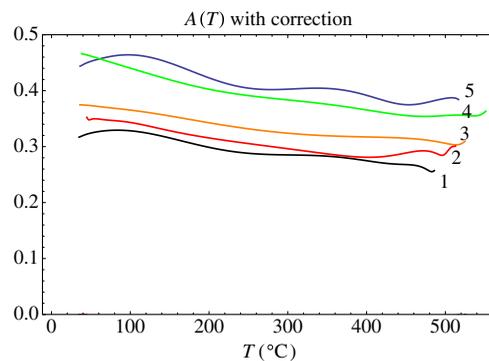

Fig. 10 Measured absorptivity of one Al sample undergoing consecutive heating and cooling cycles up to ~550°C. The numbers 1 to 5 denote the thermal cycle for that measurement. The increase in absorptivity after each thermal cycle is evidence for the modification of the oxide layer in Al. The sample was illuminated at 24 W/cm².
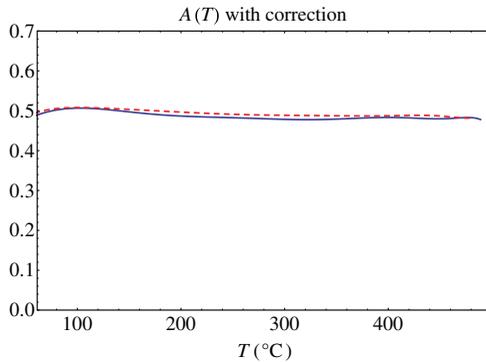
Fig. 11 Measured Ti absorptivity in two consecutive heating and cooling experiments. High repeatability suggests that no significant surface modification occurred under the test conditions.

~580°C, slight surface modifications were noticeable and an increase in absorptivity was found after cooling the sample (cf. Fig. 10). A probable source for this increase is the modification of the oxide layer. The increase in absorptivity after each thermal cycle is evidence for the modification of the oxide layer in Al. Figure 8 shows that an increase of the oxide layer thickness from 50 to 70 nm is sufficient to explain the results. Modification of surface roughness and defect generation also may be factors.

4 Absorptivity of Titanium and Steel

Measurements on Ti-6Al-4V samples were performed in a similar manner. The temperature distribution over the samples was uniform, and readings of all thermocouples were very similar. Uniform changes in the metal color caused by irradiation were observed, but these did not affect the measured absorptivity of approximately 0.5 and was only weakly dependent on the temperature as shown in Fig. 11.

Absorptivity measured for 4130 steel on as-received samples was close to 0.5, nearly independent of temperature up to $T \sim 300°C$, and was generally increasing, though not uniformly, above this temperature. After the initial test, discolored spots could be seen on the sample surface, which may be attributed to oxidation (cf. Fig. 12). After cooling to room temperature, absorption measured on the already oxidized surface was about 0.8, higher than the as-received sample up to about 400°C and then was approximately the same at higher temperatures. Temperature variations over the
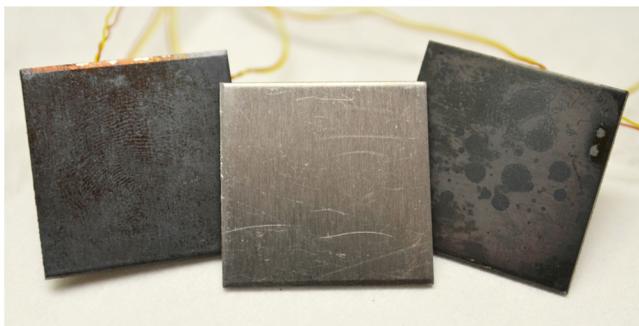

Fig. 12 Steel oxidizes and changes color after irradiation. Seen at center is a fresh sample of steel 4130. The sample on the right was heated by direct laser illumination to ~800°C and discolored spots are clearly observed on the surface. The sample on the left had been used in several such tests the previous day now shows signs of rust on the surface.
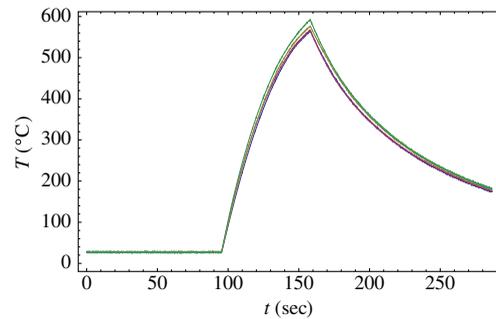

Fig. 13 Thermocouples readings on a steel 4130 sample in the heating and cooling experiments. The difference in thermocouple readings is due to uneven surface oxidation.

sample's surface resulting from changes in absorptivity at various locations on the surface due to oxidation were observed, as shown in Fig. 13. As a result, absorptivity is calculated using the mean temperature measured by the thermocouples and is shown in Fig. 14. Let us mention that the absorptivity increase measured during the initial illumination may be partially explained by the heat released during the oxidation process.

As a comparison, we also tested stainless steel 316, which possesses higher resistance to corrosion and oxidation, under similar conditions and observed little absorptivity change in multiple heating and cooling cycles up to 500°C, as shown in Fig. 15. In particular, the sudden onset of surface modification at ~400°C observed in steel 4130 is not present in stainless steel 316. Visible surface discoloration was observed in stainless steel 316 when samples were heated to over 600°C, likely as a result of surface oxidation. More detailed studies at higher temperatures are desired.

Note that, to the best of our knowledge, most of the previous measurements were done using relatively small laser spots where the effect of nonuniform oxidation may be overlooked. The importance of oxidation and its nonuniformity makes the absorptivity sensitive to the environment. For example, airflow, which affects oxidation,[2,8] can increase absorptivity. The oxidation process also releases additional energy which, in our experiments, can be counted as enhanced absorptivity.

5 Thermal Losses

Thermal loss consists of two primary components: convective cooling and thermal radiation. At low temperatures, radiative loss is small and can be disregarded. The heated surface induces convective flow near it, which cools the sample. Convective flow near a vertical wall is characterized by the Grashof number, Gr,

$$\mathrm{Gr} = \frac{\beta g x^3 \Delta T}{\nu^2} = \frac{g x^3 \Delta T}{\nu^2 T}, \qquad \beta = -\frac{\partial \rho}{\rho \partial T} \approx \frac{1}{T}. \qquad (3)$$

Here g is the gravitational acceleration, ν is the air kinematic viscosity, x is the sample size, and ΔT is the difference between the sample temperature T and the ambient temperature. For the developed convection, $\mathrm{Gr} \gg 1$. In our case, for $x = 3$ cm, $\Delta T = 100$, and $T = 400$ K, $\mathrm{Gr} \sim 10^5 \gg 1$. The cooling flux is given by the expression

A(T) of steel 4130, sample 1
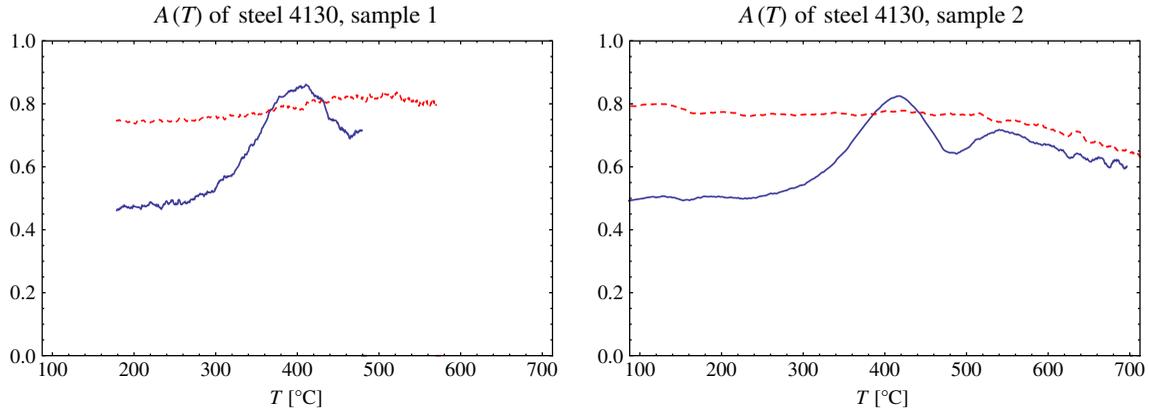
A(T) of steel 4130, sample 2

Fig. 14 Measured $A(T)$ for two steel 4130 samples under illumination of 12 W/cm² (a) and 24 W/cm² (b). The solid (blue) curve corresponds to the first thermal measurement cycle and dashed (red) curve for the same sample under a second illumination at same irradiance.

$$P_T = \frac{\kappa}{x} \mathrm{Nu} \Delta T, \tag{4}$$

where κ is the air heat conduction and Nu is the Nusselt number. For our range of Gr, $\mathrm{Nu} = (1/2)[\mathrm{Pr}^{1/2}/(0.95 + \mathrm{Pr})^{1/4}]\mathrm{Gr}^{1/4}$.[8] Here, Pr is the Prandtl number, the ratio of viscosity to the thermal diffusivity, which for air is Pr ~ 0.7. Note that viscosity and thermal conduction vary with temperature

$$\nu = \nu_0 (T/T_0)^{3/2}, \qquad \kappa = \kappa_0 (T/T_0)^{1/2}. \tag{5}$$

The above value of the Nusselt number was obtained for experiments with the temperature independent viscosity and thermal conduction. Our data are fitted using the same Eq. (4) with viscosity and thermal conduction taken at the sample temperature and an adjustable numerical coefficient c. Thus, the thermal flux, after averaging over the plate, can be represented as

$$P_T = 2c \cdot 0.5 \kappa_0 \Delta T \left(\frac{g}{x \nu_0^2} \right)^{1/4} \left(\frac{T_0 \Delta T}{T^2} \right)^{1/4}. \tag{6}$$

Here, the factor 2 accounts for convection losses from each side of the sample. At room temperature,
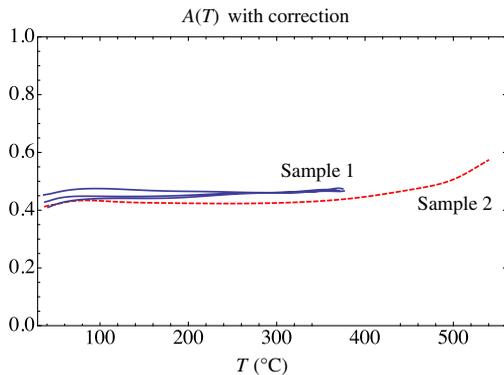
A(T) with correction

Fig. 15 Measured $A(T)$ for two samples of stainless steel 316 under 12 W/cm² illumination. The solid (blue) curves are from three consecutive thermal cycles on the same sample. The dashed (red) curve is from a second sample heated to higher temperature, showing consistent results between samples.
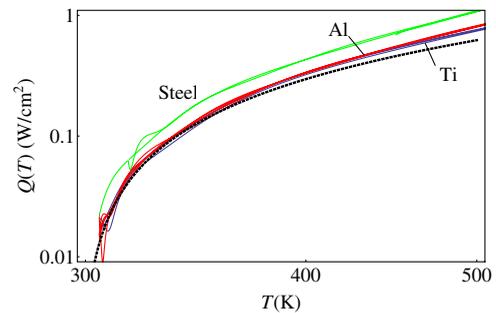
$\kappa_0 = 2 \times 10^{-4}\,\mathrm{W\,cm^{-1}\,K^{-1}}$ and $\nu_0 = 0.157\,\mathrm{cm^2/s}$. For $x = 3$ cm

$$P_T \approx 2.3 \times 10^{-3} c \Delta T \left(\frac{T_0 \Delta T}{T^2} \right)^{1/4} \frac{\mathrm{W}}{\mathrm{cm^2 K}}. \tag{7}$$

Comparison of Eq. (7) with $c = 1.9$ and experimental data for Al, Ti, and steel samples are shown in Fig. 16. At low temperatures, Eq. (7) provides a good description of convective losses and the losses for Al and Ti are similar. The convection losses are independent of materials. At higher temperatures, losses are expected to exceed those given by Eq. (7) due to radiative losses and will be discussed later.

The above estimates were made for steady-state convection. It can be different in a nonstationary regime. Let us estimate the time for a steady-state flow onset. Heat diffuses from the sample surface to the air over the distance $\delta \sim \sqrt{Dt}$, inducing a convective flow with the velocity u. In a convective flow, buoyancy is compensated by viscosity

$$\frac{\nu u}{\delta^2} \sim g\beta \Delta T, \qquad u \sim \frac{g\beta \Delta T D t}{\nu}. \tag{8}$$

In a steady state, the vertical temperature convection is compensated by the lateral thermal transport

Fig. 16 Measured thermal losses $Q(T)$ for several experimental tests on Al (red), Ti (blue), and steel 4130 (green) samples. Dashed line represents an estimate for convective cooling in accordance with Eq. (7).
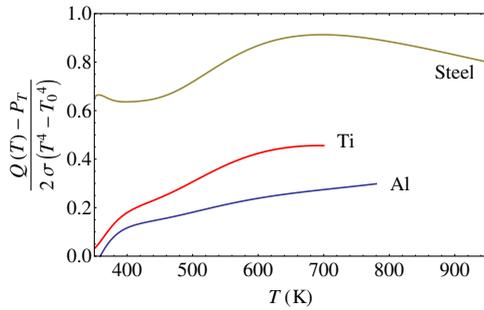
$$\varepsilon = \frac{\int I_\lambda \mathrm{d}\lambda \mathrm{d}\Omega}{\int I_{\mathrm{bb}}(\lambda)\mathrm{d}\lambda \mathrm{d}\Omega} = \frac{\int I_\lambda \mathrm{d}\lambda \mathrm{d}\Omega}{\sigma T^4 - \sigma T_0^4}. \qquad (12)$$

The emissivity is related to the absorptivity and sensitive to the surface quality and the change from sample to sample. As a result, there is considerable variability in emissivity data.[8] In our specific case, the emissivity can be estimated by

$$\varepsilon = 0.5 \frac{Q(T) - P_T}{\sigma T^4 - \sigma T_0^4}. \qquad (13)$$

The graph of emissivity for Al, Ti, and steel calculated from Eq. (13) is shown in Fig. 17. The data have been averaged over a few samples. It should be noted that the data variation from sample to sample is not small—larger than 20%. Nevertheless, the result is consistent with Fig. 16—steel radiates more than Ti and Ti more than Al. Let us estimate the radiative losses for Al. The blackbody radiation losses at 500°C are about 4 W/cm². If we use an emissivity of about 0.25 from Fig. 17, the total radiative losses at 500°C would be ~1 W/cm² of the total losses of ~3 W/cm² from Fig. 5.

6 Conclusion

To the best of our knowledge, the first measurements of absorptivity of 0.8-μm light by engineering grade metals over a broad temperature range are presented. The measurements were performed utilizing a simple calorimetric setup. Use of laser diodes as a light source makes possible the uniform irradiation of large samples. The direct measurement approach simplifies the data processing and allows for accurate determination of absorptivity. Thermal losses due to convection and thermal radiation are shown to play an important role in energy balance and must be taken into account. A method to subtract thermal losses to derive absorptivity at elevated temperatures is demonstrated. It was found that up to a temperature of ~450°C, the absorptivity of Al 6061 varies weakly with temperature, consistent with measurements at 1.3 μm (Ref. 3) and almost two times higher than absorptivity at 1 μm². This result is expected due to the interband transition peak near 825 nm. The absorptivity of Ti-6Al-4V is also insensitive to the temperature and comparable with absorptivity at 1 μm. Measurements of steel 4130 show that oxidation can affect absorptivity. As oxidation occurs nonuniformly over the sample, the local absorptivity also varies and one can only talk about average absorptivity values. Evaluation of the thermal losses, which may be derived from our measurements, also provides useful information about convective and radiative losses. Finally, methods presented here can be applied in measurements of absorptivity for a variety of materials using laser diodes or other laser sources with different wavelengths.

Fig. 17 Emissivity calculated from Eq. (12) for several metal alloys: Al 6061 (blue), Ti-6Al-4V (red), steel 4130 (brown).

$$\frac{u\Delta T}{x} \sim \frac{D\Delta T}{\delta^2}. \qquad (9)$$

Combining the last two equations, one gets for the onset time

$$t \sim \sqrt{\frac{\mathrm{Pr}\, x}{g\beta\Delta T}} = \sqrt{\frac{\mathrm{Pr}\, xT}{g\Delta T}}. \qquad (10)$$

For $T \sim 300$°C, $x = 3$ cm, and Pr ~0.7 in air, the onset time is small, $t \approx 0.06$ s. Practically, the convection is expected to be in a stationary regime. This conclusion is consistent with the absorptivity results that were measured for different pump intensities.

Now, with an estimate for the convective loss, one can subtract it from $Q(T)$ and obtain the contribution from radiative losses. Convective losses are independent of the material but sensitive to the sample geometry. Radiative losses are independent of geometry but are sensitive to the material. Data for Al and Ti will be presented.

The intensity of thermal radiation according to Kirchhoff's law can be related to the blackbody radiation $I_{\mathrm{bb}}(\lambda)$ and reflectivity R_λ[8]

$$I_\lambda = \varepsilon_\lambda I_{\mathrm{bb}}(\lambda) = (1 - R_\lambda) I_{\mathrm{bb}}(\lambda). \qquad (11)$$

Total emissivity is obtained after averaging over all angles and wavelengths
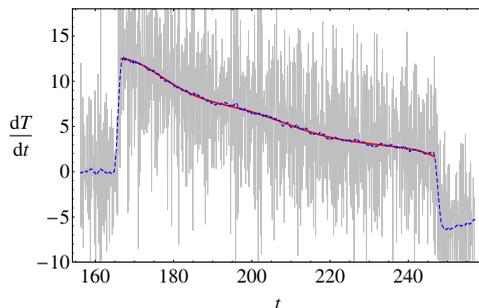

Fig. 18 Comparison of traces produced by direct differentiation of measured temperatures (gray), 21 point quadratic Savitzky–Golay derivative filter (blue), tenth-order polynomial fit of measured data followed by differentiation (red).

Appendix A

Differentiation of noisy experimental data is typically unreliable, so we describe two smoothing techniques: least-squares polynomial fit and Savitzky–Golay derivative filter. Since the temperature signal is a well-behaved monotonic function during heating and cooling, finding least-squares polynomial fits for the recorded data over the heating and

cooling periods is simple and produces fairly good approximations. We found tenth-order polynomial fits to the measured data followed by differentiation in some of our thermal calculations. In other cases, we utilized the method of least squares described by Savitzky and Golay,[9] where a given number of data points are fitted to a low-order polynomial via a least-squares procedure to obtain the value of the smoothing interpolant at the center of the interval. The least-squares calculations may be carried out by convolution of the data points with properly chosen sets of integers. This method assumes that the data are evenly spaced and without breaks. Due to technical issues, our recorded time series data usually contain uneven spacing and short breaks where no useful data are recorded. This poses no problems for the polynomial fit algorithm but offers some complications when one tries to directly apply Savitzky–Golay filters. Because in most cases the simplistic polynomial fit agrees very well with the approximation found via the more sophisticated Savitzky–Golay method, as seen in Fig. 18, these methods were applied interchangeably and without distinction where appropriate.

Acknowledgments

References

1. E. D. Palik, *Handbook of Optical Constants of Solids*, Academic Press, San Diego, California (1998).
2. A. M. Prokhorov et al., *Laser Heating of Metals*, Adam Higler, Bristol (1990).
3. R. K. Freeman, F. A. Rigby, and N. Morley, "Temperature-dependent reflectance of plated metals and composite materials under laser irradiation," *J. Thermophys. Heat Transfer* **14**(3), 305–312 (2000).
4. K. G. Mills, *Recommended Values of Thermophysical Properties for Selected Commercial Alloys*, Woodhead Publishing, Cambridge, England (2002).
5. S. Krishnan and P. C. Nordine, "Optical properties of liquid aluminum in the energy range 1.2–3.5 eV," *Phys. Rev. B* **47**(18), 11780–11787 (1993).
6. S. Krishnan and P. C. Nordine, "Analysis of the optical properties of liquid aluminum," *Phys. Rev. B* **48**(6), 4130–4131 (1993).
7. L. Landau and E. Lifshitz, *Electrodynamics of Continuous Media*, Pergamon Press, Oxford, UK (1960).
8. E. Eckert and R. Drake, *Analysis of Heat and Mass Transfer*, McGraw Hill, New York (1972).
9. A. Savitzky and M. Golay, "Smoothing and differentiation of data by simplified least squares procedures," *Anal. Chem.* **36**(8), 1627–1639 (1964).

Alexander M. Rubenchik received his PhD degree in theoretical physics from the Institute of Nuclear Physics, Novosibirsk, in 1974, and the Dr. Sci. degree from the Space Research Institute, Moscow, in 1983. Since 1992, he is a physicist at Lawrence Livermore National Laboratory at Livermore. His main scientific interests are in physics of laser-matter interactions, nonlinear optics including the studies of optical damage, laser physics and plasma physics. He has over 350 publications, 4 100 R&D awards. He is a member of OSA and DEPS.

Sheldon S. Q. Wu received his PhD degree in electrical engineering with specialization in photonics from the University of California at San Diego in 2009. Since then, he has conducted ongoing research in the NIF & Photon Science Directorate at Lawrence Livermore National Laboratory. He has made technical contributions in the fields of diode-pumped alkali lasers and precision Compton scattering light sources for nuclear photonics applications. His main scientific interests are laser physics, laser-matter interactions, classical and quantum electrodynamics, high field physics, and quantum optics.

Biographies of the other authors are not available.